Geochemistry, Geophysics, Geosystems®

AGU ADVANCING EARTH AND SPACE SCIENCE

RESEARCH ARTICLE
10.1029/2022GC010462

Unraveling the Magnetic Signal of Individual Grains in a Hawaiian Lava Using Micromagnetic Tomography

Martha E. Kosters[1], Rosa A. de Boer[1], Frenk Out[1], David I. Cortés-Ortuño[1], and Lennart V. de Groot[1]

[1]Paleomagnetic Laboratory Fort Hoofddijk, Department of Earth Sciences, Utrecht University, Utrecht, The Netherlands

Key Points:

- We studied a sample from the 1907-flow of Kilauea (Hawaii) with well-known rock-magnetic properties using Micromagnetic Tomography (MMT)
- We performed 16,874 MMT inversions to characterize the magnetic moments of 1,646 grains, resulting in 261,305 magnetic moments
- Magnetic moments were found only for grains >1.5–2 μm that exhibit multidomain behavior, but these MMT results are statistically robust

Supporting Information:

Supporting Information may be found in the online version of this article.

Correspondence to:

M. E. Kosters,
m.e.kosters@uu.nl

Citation:

Kosters, M. E., de Boer, R. A., Out, F., Cortés-Ortuño, D. I., & de Groot, L. V. (2023). Unraveling the magnetic signal of individual grains in a Hawaiian lava using Micromagnetic Tomography. *Geochemistry, Geophysics, Geosystems*, *24*, e2022GC010462. https://doi.org/10.1029/2022GC010462

Received 4 APR 2022
Accepted 5 OCT 2022

Abstract Micromagnetic Tomography (MMT) is a new technique that allows the determination of magnetic moments of individual grains in volcanic rocks. Current MMT studies either showed that it is possible to obtain magnetic moments of relatively small numbers of grains in ideal sample material or provided important theoretical advances in MMT inversion theory and/or its statistical framework. Here, we present a large-scale application of MMT on a sample from the 1907-flow from Hawaii's Kilauea volcano producing magnetic moments of 1,646 grains. We produced 261,305 magnetic moments in total for these 1,646 grains, an increase of three orders of magnitude compared to earlier studies to assess the robustness of the MMT results, and a major step toward the number of grains that is necessary for paleomagnetic applications of MMT. Furthermore, we show that the recently proposed signal strength ratio is a powerful tool to scrutinize and select MMT results. Despite this progress, still only relatively large iron-oxide grains with diameters >1.5–2 μm can be reliably resolved, impeding a reliable paleomagnetic interpretation. To determine the magnetic moments of smaller (<1 μm) grains that may exhibit pseudo-single domain behavior and are therefore better paleomagnetic recorders, the resolution of the microcomputed tomography and magnetic scans necessary for MMT must be improved. Therefore, it is necessary to reduce the sample size in future MMT studies. Nevertheless, our study is an important step toward making MMT a useful paleomagnetic and rock-magnetic technique.

Plain Language Summary The magnetic information of volcanic rocks is an invaluable archive of the behavior of the Earth's magnetic field through time. Recently, a new technique, Micromagnetic Tomography, was proposed that promises to determine the magnetic signals of individual iron-bearing grains in these rocks. This would greatly improve our ability to obtain and interpret the magnetic information stored in them. Here, we go beyond the proof-of-concept of this exciting new technique and show that it is indeed possible to obtain statistically robust results for a set of rather large grains, with diameters >1.5–2 μm, in a sample from the 1907-flow from Hawaii's Kilauea volcano.

1. Introduction

Geological materials and archeological artifacts containing magnetic particles record the direction and intensity of the past geomagnetic field as they cool. These thermoremanent magnetizations are our primary source of information on the behavior of the Earth's magnetic field. Obtaining reliable paleointensities and paleodirections from samples with a large variation in grain sizes is a challenge due to differences in magnetic behavior between grains that differ in size, shape, and chemistry (e.g., Dunlop & Özdemir, 1997; Tauxe & Yamazaki, 2015). In paleomagnetic measurement techniques that rely on bulk measurements, the contributions of individual grains are measured collectively, that is, the signals of many millions of grains result in a single magnetic moment for the entire sample. This possibly obscures information from grains that record the paleofield well by the signal of nonperfect recorders in the sample. Especially, the presence of large (>>1 μm), multidomain (MD) grains often prevents a reliable interpretation of a magnetic signal from a bulk sample. Samples consisting of predominantly single-domain (SD) grains or slightly larger (<1 μm) pseudo-single domain (PSD) grains with complex domain structures such as vortices or "flower states" generally produce more reliable paleomagnetic data (e.g., Nagy et al., 2017, 2019).

Over the past decades, a number of studies have focused on high-end magnetometry techniques to assess the magnetic state of magnetic recorders and micromagnetic processes in them on a (sub) micrometer scale (e.g., Almeida et al., 2016; Farchi et al., 2017; Lima & Weiss, 2009; Nichols et al., 2016; Weiss et al., 2007). These magnetometry techniques, such as scanning SQUID microscopy (Egli & Heller, 2000; Lima & Weiss, 2016;

Weiss et al., 2007), Electron Holography (Almeida et al., 2016; Feinberg et al., 2006; Harrison et al., 2002), and the Quantum Diamond Microscope (QDM; Fu et al., 2020; Glenn et al., 2017; Levine et al., 2019) allow to zoom in on individual grains or magnetically well-behaved small regions in a sample, and thus can avoid magnetically adverse behaved regions or grains.

The recently developed Micromagnetic Tomography method (MMT; de Groot et al., 2018, 2021) builds on this collection of magnetometry techniques. MMT proposes to overcome the differences in recording properties between grains of various sizes in a bulk sample by separating the contributions of individual grains to the bulk magnetic signal from the bulk signal. It relies on supplementing the results of scanning magnetometry on the surface of a sample with spatial data of the magnetic recorders within a nonmagnetic matrix. This enables a three-dimensional interpretation of the magnetometry results through a least squares inversion that allocates magnetizations to individual magnetic grains. The spatial data on the magnetic recorders are acquired from X-ray microcomputed tomography (MicroCT) scans.

As recognized by de Groot et al. (2021), the development of MMT is promising, but currently there are major challenges left to solve before MMT can be routinely used for paleomagnetic and rock-magnetic studies. Most previous MMT studies used synthetic samples and produced results for a limited number of grains (<150). Here, we present the first results from MMT applied to a natural volcanic sample. We show (a) that it is possible to determine magnetic moments for large, MD, grains, (b) that the current computational setup is capable of solving for a statistically relevant number of grains, and (c) which challenges currently remain to obtain useful paleomagnetic and rock-magnetic information. Despite our progress, our MMT results cannot yet be interpreted in paleomagnetic terms because we only solve for the moment of large, MD, grains. To obtain information from the paleomagnetically more relevant, PSD, grains, the resolution of the MicroCT scan must be increased. Nevertheless, our study provides an insight into how the development of MMT for paleomagnetic uses can progress, and we illustrate how MMT data can be scrutinized and selected based on the recently proposed statistical framework by Out et al. (2022).

2. Sample Description

For this study, we selected material from the 1907 lava flow of Kilauea, Hawaii. This material was sampled as site HW03 (de Groot et al., 2013), and its rock-magnetic properties were described in depth (ter Maat et al., 2018). Our sample is a cylindrical cutout from a thin section with a sample layer of 30 μm thick, with a diameter of 3 mm. The same sample was used as one of the case studies in de Groot et al. (2021). HW03 consists of tholeiitic basalt with minor alterations, consisting of a low percentage (<5%) of iron-oxides.

2.1. Petrography

The iron-oxides are copious and distributed throughout the sample. They are <30 μm in size, have a cubic shape and have experienced minor oxyexsolution (Figure 1 and ter Maat et al., 2018). A micrograph of the thin section shows that the sample contains areas dominated by fewer, relatively large iron-oxide grains (>3 μm, "A" in Figure 1a) and areas dominated by a higher number of relatively small (<3 μm, "B" in Figure 1a) iron oxide grains. The circular cut-out that was used for this study contains an area with mainly relatively large grains, and thus not many of them. The material surrounding the iron-oxide grains has a porphyritic structure with large (100–200 μm) clinopyroxene and plagioclase crystals and contains some equant olivine phenocrysts. The remaining material mainly consists of fine-grained clinopyroxene, plagioclase, and glass (Figures 1b–1d).

2.2. Chemical and Magnetic Analysis

ter Maat et al. (2018) performed a chemical analysis of 22 iron-oxide grains from HW03 using a microprobe. Based on the microprobe analysis, the iron-oxide grains can be roughly divided into two mineralogical families. The first mineralogical family is ilmenite with a relatively equal Ti and Fe content of ∼19 atom% each (6 grains). The other family is titanomagnetite with a high Fe and low Ti content varying in ratio from 3:1 to 7:1 (15 grains). Lastly, there is one grain of which two spot readings show that it is partly ilmenite and partly titanomagnetite. Further investigation using Scanning Electron Microscope using Backscatter Electrons to characterize the crystallographic lattice shows mineralogical domains within grains that are either titanomagnetite (cubic) or

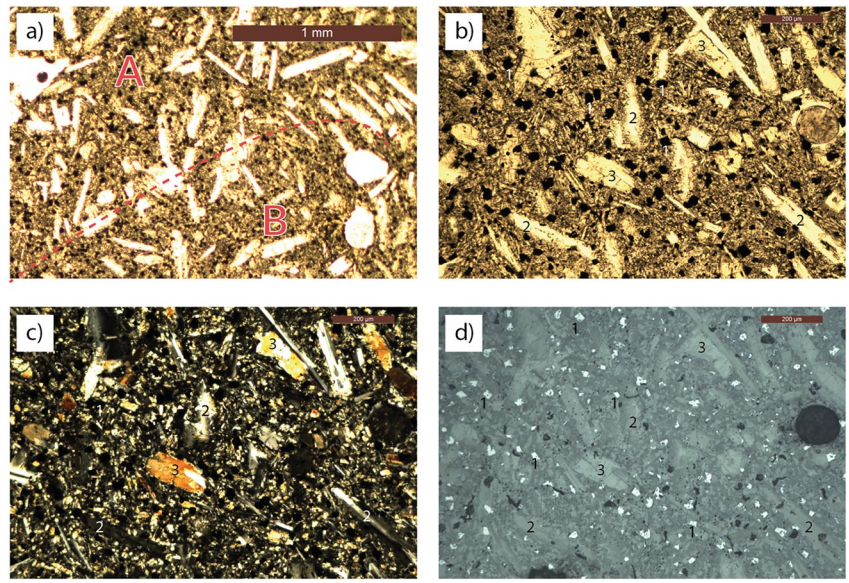

Figure 1. Petrology and mineralogy of HW-03. Panel (a) shows a portion of the sample under plane polarized light (PPL) in which two areas A and B are loosely defined. Area A is an area with a sparse number of large magnetite grains and area B is an area with a higher density of smaller magnetite grains. The magnification in panels (b–d) is larger and shows the sample under PPL, crossed polarized light and reflected light, respectively. Each shows the same field of view in which the different minerals are indicated: magnetite (1), clinopyroxene (2), and plagioclase (3). The cubic nature of the magnetite grains is especially visible under reflected light (d).

ilmenite (hexagonal). Within these mineralogical domains, magnetic domains can exist, but it is important to keep in mind that the Curie temperature of titanomagnetite decreases with increasing Ti content, from 580°C for the magnetite ($x = 0$) endmember to below room temperature for high-Ti compositions ($x > 0.8$). The ilmenite endmember is paramagnetic at room temperature (Readman & O'Reilly, 1972), that is, only the titanomagnetite grains may hold a remanent magnetization. Investigation by Magnetic Force Microscopy (MFM) of four grains indeed showed multiple magnetic domains within the titanomagnetite mineralogical domains (ter Maat et al., 2018) but no magnetic signal in the ilmenite part of these particular grains. As it is currently impossible to discriminate between ilmenite and titanomagnetite in the MicroCT scans used to characterize the iron-oxides for our MMT study, some (parts) of the grains selected by the MicroCT analyses do not have a magnetic signal at room temperature.

3. Methods

The MMT method relies on combining spatial information of the position and shape of individual magnetic grains with the magnetic flux density map of those same grains to solve their individual magnetic moments (de Groot et al., 2018, 2021). Supplementing the magnetic scan with spatial information is necessary to overcome the traditional nonuniqueness in potential field inversion problems (Fabian & de Groot, 2019).

3.1. Spatial Data Acquisition

The spatial information is derived from MicroCT scans that produce a three-dimensional image of the X-ray attenuation contrast in a sample that is often interpreted in terms of variations in density in the sample (e.g., Sakellariou et al., 2004). The interpretation of the three-dimensional image relies on the large attenuation contrast between the highly dense magnetic grains and the lower density surrounding matrix. Using a threshold, voxels with high density are retained and those with low density are removed. Subsequently, adjacent, interconnected, high-density voxels are grouped together to form a grain, for which the size, shape, and position are known. From these data, physical properties such as volume and the distance to the surface can be calculated for each grain individually. The sample for this study was imaged by the Nanotom-S MicroCT at TU Delft. The scan has a resolution of 0.75 μm (voxelsize: 0.75 μm × 0.75 μm × 0.75 μm) and a field of view of 1,901 × 2,301 pixels. To

suppress noise, grains that consist of 10 voxels or less were discarded, which inherently implies that the smallest grains included in the inversion routine are approximately 1.5–2 μm in diameter. This is a major shortcoming of our MMT study, as smaller grains are undoubtedly present in our sample and are assumed to be the most reliable magnetic recorders. Also, it is important for the inversion routine that all magnetic sources in the system are known, otherwise there are magnetic contributions in the surface magnetometry that cannot be attributed to their source. Missing grains with diameters <1.5–2 μm will therefore lead to less reliable MMT results. Nevertheless, the mineralogical investigation of this sample shows that many grains in our sample are >3 μm. Furthermore, a major part of the discussion of this paper consists of assessing how well the grains that are detected by our MicroCT scan are resolved, in spite of missing smaller grains in our sample and other sources of uncertainty.

3.2. Magnetic Flux Density

The magnetic flux density map required for MMT can be imaged using a variety of instruments and techniques (as summarized in de Groot et al. (2021)). The sample in our study was imaged by a QDM at Harvard (Glenn et al., 2017). The QDM determines the magnetic flux density above the surface of a sample by measuring dips in the magnetic field-sensitive fluorescence of nitrogen-vacancy centers in a diamond chip (i.e., in the sensor). The magnetic data is thus acquired from an optical image with a field of view of 1,920 × 1,200 pixels and a spatial resolution of 1.2 μm. During the operation, a 0.9 mT bias field is applied; its polarity is switched many times during measurement. Induced (paramagnetic) magnetization in the sample can be removed from the remanent (ferrimagnetic) part of the signal by taking the average of the images acquired with switched polarity. For a more detailed explanation of the operation of the QDM, we refer to (Glenn et al., 2017) and (Levine et al., 2019). The coercivities of naturally occurring SD and PSD iron-oxide grains are generally >>0.9 mT (Dunlop & Özdemir, 1997; Readman & O'Reilly, 1972); for MD iron-oxide grains the coercivity will be lower but most likely still >0.9 mT. The QDM's bias field should therefore not prevent a paleomagnetic interpretation of QDM results. If grains have coercivities <0.9 mT, they are most likely close to superparamagnetic, in which case they are not reliable recorders of the paleofield anyway. In future studies, the effect of the bias field can be determined as we move to smaller resolutions and are able to image more PSD or even SD grains.

3.3. Coregistration

The two data sets (MicroCT and QDM) must be coregistered in the same coordinate system to apply the inversion routine. The QDM is an optical acquisition technique, and its camera can also be used to optically image the surface of the sample in the same coordinates as the magnetic scan. The MicroCT data can be sliced to only show the grains close to the surface of the sample. This enables coregistration based on the geometry of shallow grains (Figure 2a). Since the two scans do not overlap entirely, not all grains imaged by the MicroCT have a coregistered magnetic flux signal (Figure 2b). In total, 1,646 grains were imaged by both the MicroCT and QDM analyses. Also, the scan height, that is, the sample-sensor distance, needs to be precisely known to properly coregister the MicroCT and QDM data sets. This distance was 6.0 μm and is derived from the actuators of the QDM set-up.

3.4. Inversion Set-Up

The inversion routine is identical to the inversion scheme used in de Groot et al. (2018, 2021) and is based on the theory in Fabian and de Groot (2019). The data in those publications were processed on a desktop computer and performing the inversion routine for one tile of 150 μm × 150 μm with the same grain density would amount to ~2 weeks computational time. For this study, the inversion routine was highly optimized and moved to Python to use state-of-the-art libraries. Furthermore, we now use a computational server with 52 double-threaded cores and 192 GB RAM. These improvements allow us to perform an inversion of a single tile of 150 μm × 150 μm in approximately 1.5 min. Because the inversion has a high RAM demand, the size of the tile that can be inverted in one calculation is still limited to 150 μm × 150 μm. Therefore, the analysis of the whole sample (1,320 μm × 1,570 μm) requires a subdivision of its area into overlapping squares, called tiles, with a maximum size of 150 μm × 150 μm (Figure 2c). The tiles are interspaced by 10 μm, yielding a total of 118 × 143 = 16,874 tiles. A drawback of tiling is that grains can be intersected by the tile edge, which violates the boundary condition of the inversion that all magnetic sources in the system and their magnetic signals are imaged, and no sources or signals are missing. Tiling increasingly violates this boundary condition as grains are closer to the edge of a

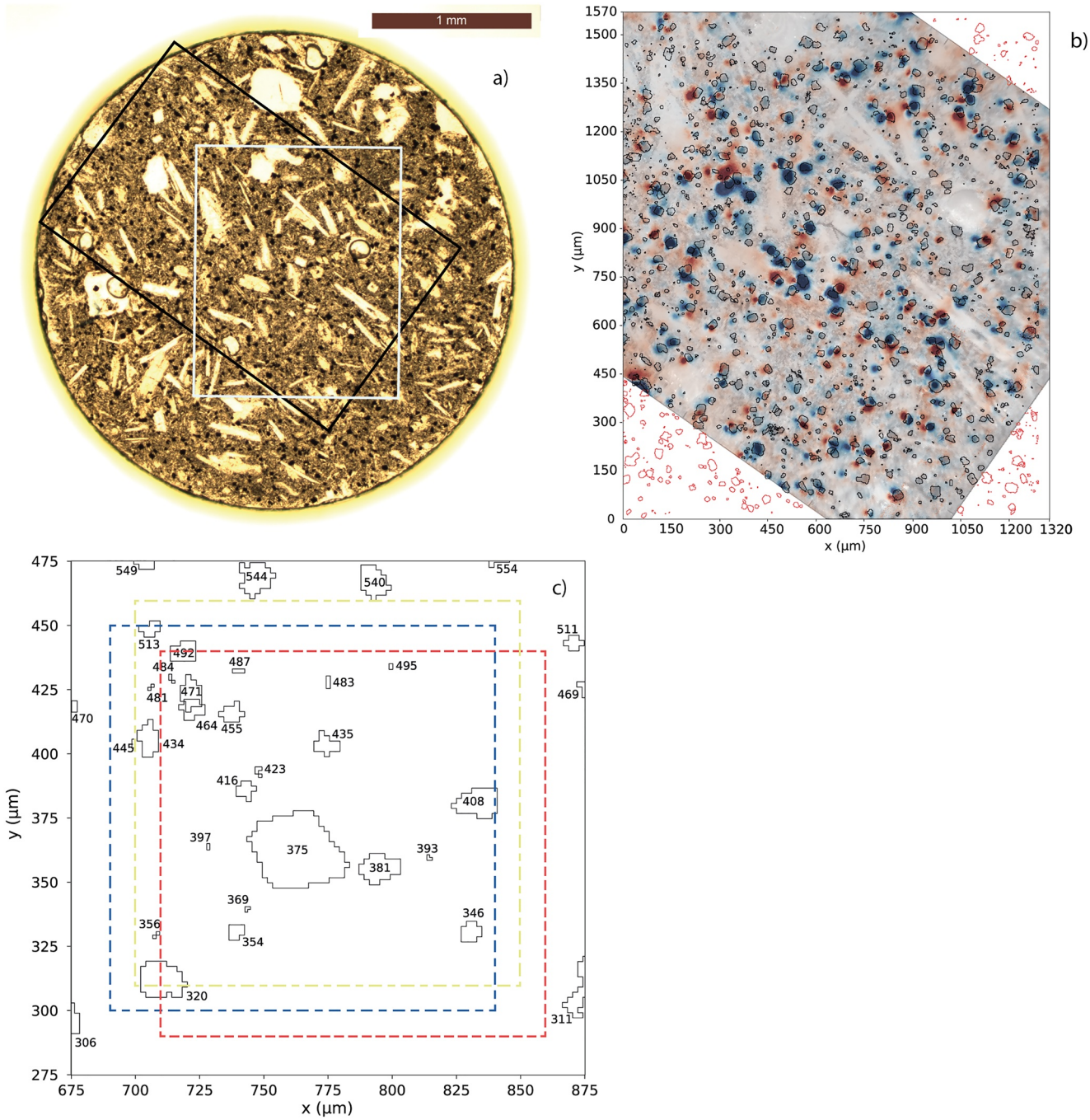

Figure 2. The mapping of the Quantum Diamond Microscope (QDM) and MicroCT-scans. Panel (a) shows a microscope image of the entire sample, with the MicroCT field-of-view outlined in white and the QDM's field-of-view in black. In panel b, the magnetic scan of the QDM is in the background (positive flux in blue, negative in red, an absolute scale lacks due to distortion from the other layer in the image), overlain by the QDM's LED image in 50% transparency. The grains as obtained from the MicroCT scan are outlined in black when they are in the QDM's field-of-view and in red when they are outside. Three unique tiles are shown in panel (c), each tile is 150 µm × 150 µm and they are spaced at 10 µm intervals. The horizontal (x) and vertical (y) axes in panels (b and c) have the same origin and are in µm. The exclusion of grains due to intersecting the boundary of a tiles is illustrated by for example, grain 513: it will be included in the blue and yellow tiles during the inversion but its results in the blue tile will be discarded after the inversion was performed because it intersects the boundary of the tile.

tile and a larger part of their signal is outside the tile. However, leaving these grains out of the inversion would likely lead to source misattribution. Thus, grains that intersect a tile edge are included in the inversion, but the result (i.e., magnetic moment) from those grains is discarded after the inversion. The advantage of tiling is that it produces multiple solutions for each grain—one for each tile that fully contains the grain—enabling a

statistical analysis of the inversion results. If the magnetic solution of a grain is robust, we expect only minor variations between the magnetic moments produced by the inversions of different tiles; if the results for a grain are dispersed, its solution is less accurate.

The inversion routine uses a least squares minimization to calculate the magnetic moment in three orthogonal directions per grain. The calculated magnetic moments and the spatial data from the grains are then used to create a calculated magnetic flux map at the sensor location in a forward model. This calculated magnetic flux map is subtracted from the original magnetic flux map to produce a map of the magnetic flux residuals, that is, the measured magnetic flux density that is not accounted for by the inversion. The inversion algorithm for a large number of magnetic particles implicitly assumes that their moments are uniquely defined by the input data. The unique source assignment theorem of Fabian and de Groot (2019) asserts that the mathematical inverse problem is well-posed even for a large number of magnetic particles, but it requires perfect knowledge of the normal field component on the boundary of the domain within which the particles are located. Real measurements determine only approximations to a finite number of these normal field components and therefore the numerical inversion method—even though well-posed in fundamental theory—may lead to ill-conditioned inverse problems. Here, our goal is to explore which fraction of the magnetizations in a real paleomagnetic sample can be reliably recovered, and which evaluation method and boundary condition are best suited to maximize this fraction.

3.5. Data Processing

Tiling leads to multiple magnetic moments for individual grains: on average there are 159 magnetic moments per grain, with a minimum of 10 and a maximum of 225 magnetic moments. From each individual magnetic moment (i.e., magnetic moment vector in three orthogonal components), the total magnetic moment (i.e., length of the magnetic moment vector), its declination with respect to the positive x-axis, and inclination with respect to the horizontal plane (downwards into the sample) are calculated. Also, for each tile, the distance to the nearest tile boundary for a grain in that tile is determined. The entire data set is subsequently grouped per grain; for each grain, we determine its mean and median magnetic moments. Furthermore, assuming Fisher statistics (Fisher, 1953), the Fisher mean, the precision parameter (k) and confidence interval ($\alpha 95$) are calculated for each grain. To assess the stability of the magnetic direction of each grain (i.e., the spread solutions from each tile in which the grain is fully present), the angle between the Fisher mean for that grain and each of its individual solutions is determined ($\Delta\alpha$). It is important to note that Fisher statistics only considers the directions of the magnetic moments, and not their magnitudes, that is, the Fisher mean has unit length. To quantify the stability of the magnetic moment of each individual grain, we calculated the percentual difference between the magnetic moment of each individual solution and the median magnetic moment for that grain (Δm). The $\Delta\alpha$ and Δm proxies can be used to investigate the stability of the results per grain between magnetic moments stemming from different tiles.

3.6. M_r/M_s Ratio

To determine whether an allocated magnetic moment is reasonable, the allocated magnetic moment is divided by the theoretical maximum magnetic moment for that grain. The theoretical maximum magnetic moment is calculated based on the saturation magnetization of pure magnetite (480 kA/m, e.g., Dunlop & Özdemir, 1997) and the volume of the grains as produced by the MicroCT analysis. This ratio is equal to the M_r/M_s ratio, as the volume factor that converts magnetic moment to magnetization is present in both the nominator and denominator and is a constant for an individual grain. The allocated magnetic moment should never be higher than the grains' theoretical M_s value. Therefore, results for which $M_r/M_s > 1$ are inherently inaccurate. Since our grains have diameters >1.5–2 μm, they are firmly outside the SD grainsize range for which a magnetic moment close to $M_r/M_s = 1$ can be expected. Realistic M_r/M_s values for individual grains are therefore well below 1, although there currently is no theoretical framework for their expected values. Furthermore, the mineralogical analyses showed that the iron-oxide grains are not pure magnetite but titanomagnetite and ilmenite. Grains with a larger percentage of Ti may have three to four times lower M_s-values compared to magnetite (Dunlop & Özdemir, 1997), and ilmenite does not hold a remanent magnetization at room temperature (Readman & O'Reilly, 1972). To make it even more complex, parts of the iron-oxide grains in our sample can be ilmenite while other parts are titanomagnetite (ter Maat et al., 2018). This makes their "magnetic grain size" smaller than the physical grain size as determined by MicroCT, lowering their expected M_r even further. All this implies that the calculated theoretical maximum magnetic moment is an absolute upper limit to the magnetic moment allocated by the inversion. For our grains, it is safe to expect M_r/M_s values to be in the order of 0.1, and possibly even (much) lower.

3.7. Signal Strength Ratio

MMT's potential to accurately resolve a grain's magnetic moment depends on (a) the magnetic signal from that grain and (b) its distance to the sensor of the magnetic scan (de Groot et al., 2018, 2021). Recently, Out et al. (2022) defined the signal strength ratio (SSR), a parameter that indicates the expected magnetic flux density at the sensor for each grain in the sample. It is based on the distance of the grains centroid to the sensor (R), volume (V), and diameter (d) and calculated by: $\mathrm{SSR} = V / R^3 d$. Furthermore, they numerically modeled the performance of MMT inversions as function of a grain's SSR and showed that the SSR can be used to select a subset of grains of which a predefined percentage of grains produces an accurately resolved magnetic moment. The proper SSR cut-off depends primarily on the noise in the magnetic scan and the concentration of grains in the sample (Out et al., 2022). It must be noted that the numerical study by Out et al. (2022) does not have a sample-sensor height, and it remains to be investigated if and how this affects the SSR cut-off.

4. Results

We inverted 16,874 tiles to characterize the magnetic moments of 1,646 grains in our sample. Due to the inversion in tiles, some grains were solved more often than others, and 261,305 magnetic moments were obtained in total. Previous MMT studies were limited to samples or tiles with <150 grains that were inverted only once (de Groot et al., 2018, 2021). Here, we increase the number of analyzed grains by one order of magnitude and the number of individual magnetic moment estimates by three orders of magnitude. Below we first present results for individual grains, then for single tiles, and lastly consider the entire sample—including selecting the grains that are best resolved in our study.

4.1. Results for Individual Grains

As each grain is included in multiple unique tiles, the magnetic moment for each grain is determined between 10 and 225 times, with 159 times as the average. In Figure 3, we present the results for three typical grains in our sample that illustrate the differences in stability between the different MMT inversions. Grain 200 is poorly resolved: there are 225 solutions, but their directions are dispersed as indicated by a precision parameter k of 1.19 (Figure 3a). Grain 319 performs better, with 180 solutions and a precision parameter (k) of 5.63 (Figure 3b). Grain 693 exhibits truly stable behavior with a k-value of 363.46 with 169 solutions (Figure 3c). We see a similar trend in the inaccuracies of the magnitude of the magnetic moments. The Δm parameter that gives the percentual difference between an individual magnetic moment and the median magnetic moment shows a tight distribution around 0% for grain 693, and increasingly flatter distributions for grains 319 and 200, respectively (Figure 3d). It is important to note, however, that the deviations in direction and magnitude are not always related, that is, not all grains for which the direction is poorly resolved produce an inaccurate magnitude as well, and vice versa (Figure 3e).

To generalize these three examples, we consider the distribution of k-values for the individual grains in our sample. Grain 319 is representative for the most common precision of the results for individual grains: the median k-value in the entire population is 4.17, with the first and third quartiles being 2.43 and 9.57, respectively. The extremes are a grain with a k-value of 1.08 on the lower end, and a grain with a k-value of 9,018.25 on the upper end.

4.2. Results for an Individual Tile

For each tile, the results consist of a list of calculated magnetic moments for the grains that are present in that tile, a calculated magnetic flux density map based on the forward model of the results produced by the inversion, and a map of the calculated residual magnetic flux. The results of a typical tile are presented in Figure 4. It contains 22 grains that are fully within this tile; another 3 are intersected by its boundary and are therefore included in the inversion, but their results are rejected. The list of solutions in this tile is in Table S1. The magnetic flux density map shows one major pattern that is not characteristically dipolar (Figure 6a, around [760,360]). Since our inversion only allocates dipoles to the individual grains, this anomaly is only partially resolved in the forward field (Figure 6b) and leaves a distinct multipolar residual (Figure 6c). The grain that is mainly beneath this multipole signal is grain 375, which is a large and shallow grain, from which MD behavior can be expected. Remarkably,

10.1029/2022GC010462

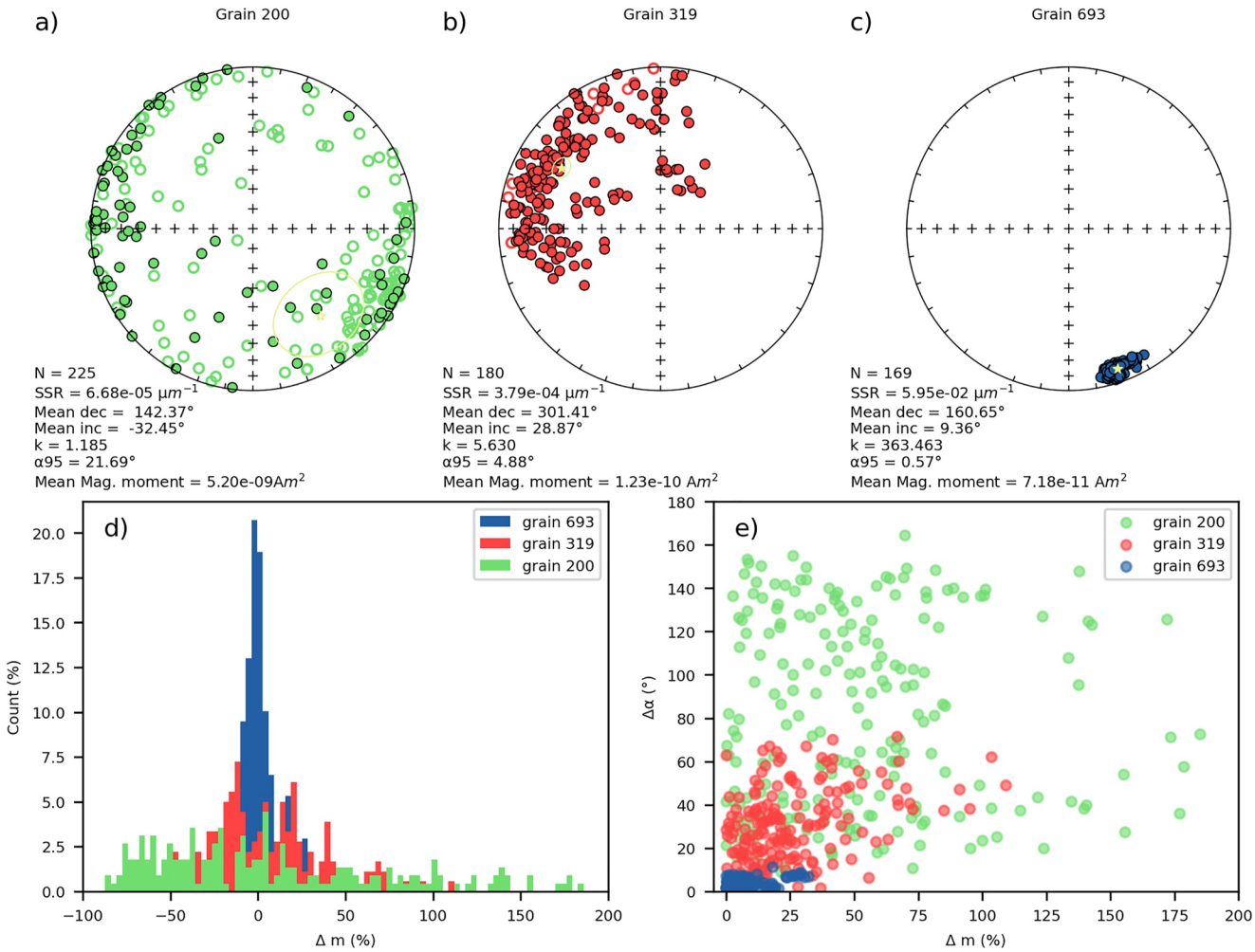

Figure 3. Results for three typical grains. Panels (a–c) show the directional results in equal area projections for grains 200, 319, and 693, respectively; closed symbols are in the lower hemisphere corresponding to positive inclinations, and open symbols are in the upper hemisphere with negative inclinations. The percentual deviation of individual magnetic moments with respect to the median magnetic moment for each grain (Δm) is in panel (d). The relationship between the angular deviation ($\Delta\alpha$) and Δm for each individual solution is in panel (e). Note that the *x*-axis in panels (d and e) is cut-off at 200% deviation; this excludes 19 individual solutions for grain 200 from the plots.

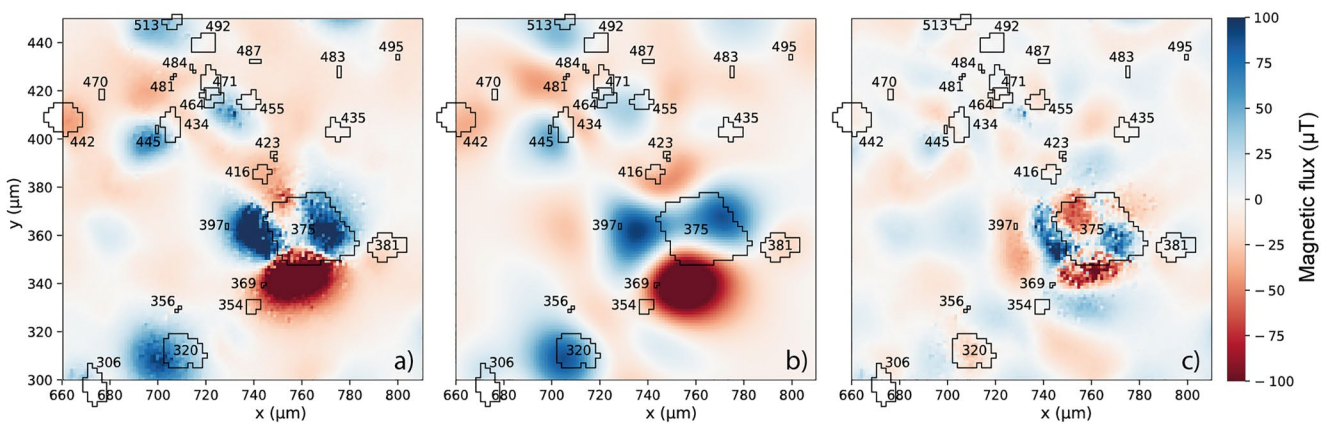

Figure 4. Example of the results of a typical tile; this tile has its lower-left corner at [660,300] and its top-right corner at [810,450] in Figure 3b. The measured magnetic flux is in panel (a); the forward field based on the allocated magnetic moments is in panel (b); and the residuals are in panel (c). The grains in the tile are outlined in black and indicated by their label (number).

the results for this grain are relatively similar for all containing tiles, leading to a narrow distribution of direction with $k = 28.43$. For many other smaller grains, the residual is low, indicating that the allocated magnetic moment is in line with the measured magnetic flux by the QDM.

4.3. Results for Entire Scanned Surface

The overlapping field-of-view of the MicroCT and QDM scans encompassed 1,646 grains for which 261,305 magnetic moments were calculated in 16,874 tiles. We already showed that the results of some grains are more stable than others, so it is paramount to select only the most reliable magnetic moments. We therefore assess the results as a function of (a) the theoretical remanence ratios (M_r/M_s) of the grains; (b) the distance to the closest edge of the tile; and (c) the SSR of the grains (Figure 5). The M_r/M_s ratio has a theoretical maximum of 1, but accurate solutions of the remanent magnetization of grains in our sample are most likely in the order of 0.1 or less (Section 3.6). Many solutions from our inversions have M_r/M_s ratios >1, but the SSR of these grains is generally low, and there is no trend between the M_r/M_s ratio of a solution and its distance to the closest edge of the tile (Figure 5a). The accuracy of the direction of the magnetic moments does show a trend with distance to the closest boundary of the tile (Figure 5b). Apparently, missing parts of the magnetic expression of a grain hampers reliable determination of the direction more than the intensity. Again, the SSR is able to discriminate between accurate and less accurate results well, but the angular deviations are still in the order of tens of degrees, even for SSRs >0.1.

5. Discussion

5.1. Mineralogy and Grain Sizes

The mineralogy of our sample was described in-depth by ter Maat et al. (2018) and studied here (Section 2). For our purposes only the iron-oxide grains in the sample are of interest, and they are abundant. To isolate the iron-oxide grains in the sample, we selected grains with high attenuation contrasts from the MicroCT scan. A high attenuation contrast is often interpreted as a material with a high density. Given the mineralogy of our sample, it is likely that the vast majority of grains with a high density are iron-oxide grains. The spatial resolution of the MicroCT scan, however, limits the size of grains that are detected to >1.5–2 μm diameter. This means that iron-oxide grains with diameters <1.5–2 μm that are undoubtedly present in our sample are missed in our analyses. Moreover, the mineralogical study of our sample shows that the chemical composition of our iron-oxide grains varies from ilmenite to (titano-)magnetite. Since ilmenite does not carry a remanent magnetization at room temperature, not all iron-oxides in our sample will have a magnetization. Some grains even have mineralogical domains, some of which are magnetic at room temperature while others are not. This implies that there are two

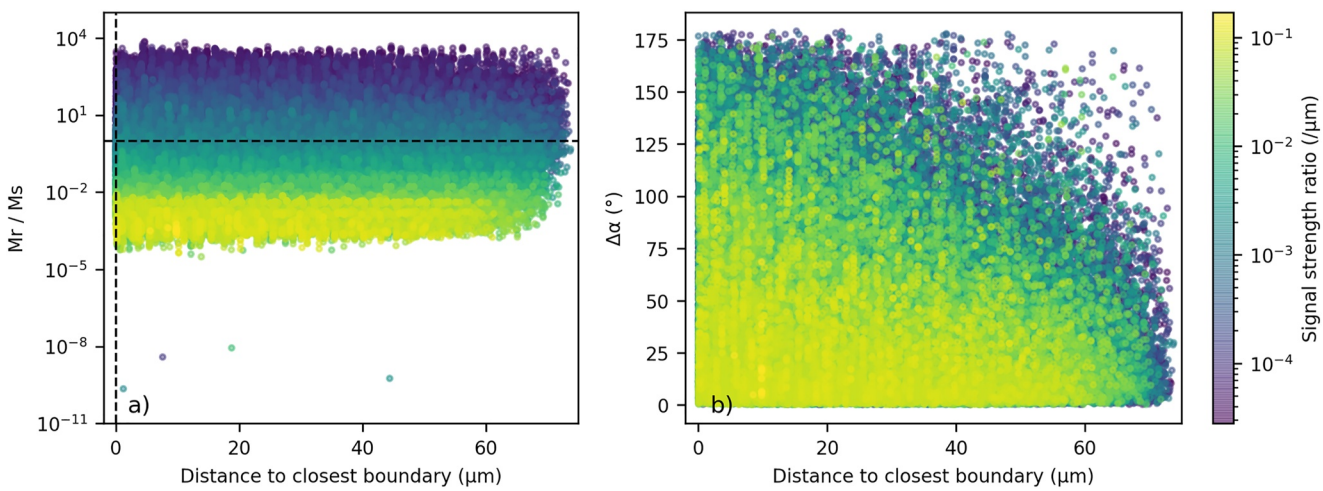

Figure 5. Accuracy of the 261,305 determined magnetic moments from 1,646 grains as a function of distance to the closest boundary of the tile and signal strength ratio (SSR). The accuracy is expressed as (theoretical) M_r/M_s ratio (a), which must be <1 and is most likely in the order of 0.1 or less; and as the angle between individual results and the mean direction of a grain ($\Delta\alpha$) in panel (b). In both panels, the results are color coded based on the SSR of the grain. Results with a theoretical M_r/M_s ratio >1 (indicated by the horizontal dashed line in panel (a)) are inaccurate as the allocated magnetization cannot be larger than the saturation magnetization.

major shortcomings in our MMT study: first, not all magnetic sources in the system are known, and second, some sources that are identified do not carry remanent magnetization. It is difficult to assess the impact of these two shortcomings, and they are subject of ongoing research. However, we expect that the impact of missing magnetic sources on the accuracy of MMT results is much larger than the impact of nonmagnetic sources in the system. Missing a source directly violates the important boundary condition of the uniqueness theorem of the inversion that states that all, but only, the magnetic sources and magnetic signals in the system must be known (Fabian & de Groot, 2019). Since the inversion can allocate a near-zero magnetic moment to a source in the system, including a nonmagnetic source in the inversions seems to be a lesser issue. In future studies, increasing the resolution of the MicroCT scan should be considered to identify as much of the iron-oxide grains in the sample as possible. The lower limit of 50 nm below which iron-oxide grains behave superparamagnetically (Dunlop & Özdemir, 1997) is challenging but not impossible for current NanoCT scanners. The field-of-view of scanners with such resolutions, however, is often narrow, limiting the volume of the sample and hence the number of grains present in a scan.

Furthermore, the variation in the mineralogy of the iron-oxides in our sample hampers our interpretation based on theoretical remanence ratios (M_r/M_s) that are based on the saturation magnetization (M_s) of pure magnetite (480 kA/m). First, the iron-oxide grains in our sample are large, multidomain, grains for which M_r/M_s ratios $<<1$ are expected. Second, the iron-oxide grains in our sample are titanomagnetites or ilmenites instead of magnetites. Since titanomagnetite has a saturation magnetization three to four times lower than pure magnetite and ilmenite is paramagnetic at room temperature (e.g., Dunlop & Özdemir, 1997; Readman & O'Reilly, 1972), the expected M_r/M_s values are lowered even further. Third, some grains have mineralogical domains of both ilmenite and titanomagnetite. Their volume as identified by the MicroCT scan does not represent their "magnetic volume" at room temperature. All this implies that the calculated M_r/M_s ratios are overestimated, and that the theoretical upper limit of 1 for the M_r/M_s ratios is too high. Therefore, we expect M_r/M_s values in the order of 0.1 or (much) less, although a theoretical framework for this value is lacking.

5.2. Geometry of MMT Experiments

A precise coregistration of the MicroCT and QDM data sets is paramount for the accuracy of MMT results. Small perturbations in the mapping between the two data sets may lead to increased uncertainties and/or poorly resolved grains in the MMT inversion. Also, the scan height—the sensor-sample distance that dictates the distance between the grains and the sensor of the magnetic scan—needs to be known with precision, as errors in this distance propagate with the power of three in MMT results (de Groot et al., 2018).

In the current workflow, the coregistration of the spatial data onto the magnetic surface scan is done by hand. This introduces an uncertainty in the mapping that may influence the results, although the grains do line up over the entire field-of-view of 1,320 μm × 1,570 μm, and there are no distortions evident over the surface (Figure 2b). The optical image of the QDM greatly eases the mapping compared to the alignment of the MicroCT scan with magnetic anomalies in the Scanning SQUID Microscopy scan as was necessary in de Groot et al. (2018). Nevertheless, the mapping is time-consuming and sometimes difficult because it is done based on the geometry of shallow grains, which have a unique pattern, but which takes time to recognize in both the LED image from the QDM set-up and the surface grains from the MicroCT scan. We briefly explored the possibility of using pattern recognition software to map the surface grains to the LED image from the QDM-setup. The amount of data that the pattern recognition can use, however, is relatively scarce because the MicroCT data consists of only the high-density grains. The results of the pattern recognition routine were not very promising; therefore, currently, the tedious process of mapping the LED image of the QDM onto the shallow grains in the MicroCT scan by hand seems to be the most accurate way of coregistration.

5.3. Multidomain Signals of Large Grains

The geometry of the magnetic flux density map of large MD grains on the sensor is often rather complex (e.g., grain 375 in Figure 4a). Since the MMT inversion that we used here only solves for dipole magnetizations in a grain, it is likely that parts of the complex magnetization of such a MD grain are attributed to surrounding grains, which are then assigned incorrect magnetizations. Even though the signal of these large MD grains may not be of interest for a paleomagnetic interpretation, solving them correctly would prevent their magnetic flux from being erroneously attributed to grains in their close surroundings. In a future study, it is therefore worth exploring

whether solving for nondipolar behavior for large grains and/or grains that are close to the scanning plane using the routines presented by Cortés-Ortuño et al. (2021) would improve the accuracy of MMT results. Special attention should be paid to select the best degree of the spherical harmonics for each grain; expanding the inversion to also solve nondipole signals most likely increases the computational time considerably. Solving for higher order degrees of spherical harmonics introduces more variables per grain, reducing the number of data points in the magnetic scan per variable to solve. Lastly, it would require a higher signal-to-noise ratio in the magnetic scan since small errors can be accommodated in more detailed descriptions of a grain's magnetization, while they would be averaged out in a dipole approximation.

5.4. Effect of the Tile Size

The tile size is limited to 150 μm × 150 μm due to RAM memory requirements. The distance to the nearest tile boundary influences the stability of the directional solution more than the stability of the length of the magnetic vector (Figure 5). To explain the dependency of the stability of the solution on the distance to the closest boundary, we determined the size of the sensor area across which the magnetic flux of a single magnetic grain is present. We therefore calculated the forward magnetic flux density of a small grain with a diameter of 2–3 μm, centroid depth of 30.76 μm, SSR = 0.00198 (grain 435) while ignoring the magnetic signals of the surrounding grains (Figure 6). The magnetic flux density map of this single grain is roughly circular with a diameter of 100 μm, it is therefore present in a major part of the tile. Larger grains will have magnetic flux density maps that encompass larger sensor areas. This implies that when using 150 μm × 150 μm tiles (major) parts of the magnetic density flux map of grains are not enclosed in the tile and are not considered in the inversion of that particular tile. This violates a boundary condition of the uniqueness theorem that stipulates that all but only the magnetic sources and their magnetic signals in the system must be known (Fabian & de Groot, 2019). It would therefore be desirable to work with larger tiles or even invert for the entire sample at once. This will be pursued in a future study, when the computational limitations currently impeding inversion of larger tiles are resolved.

5.5. Signal Strength Ratio Cut-Off

The SSR (Out et al., 2022) provides an indication of the expected magnetic flux density at the scanning plane for each grain based on its size and location in the sample. The SSR is thus a first-order estimate of the signal-to-noise

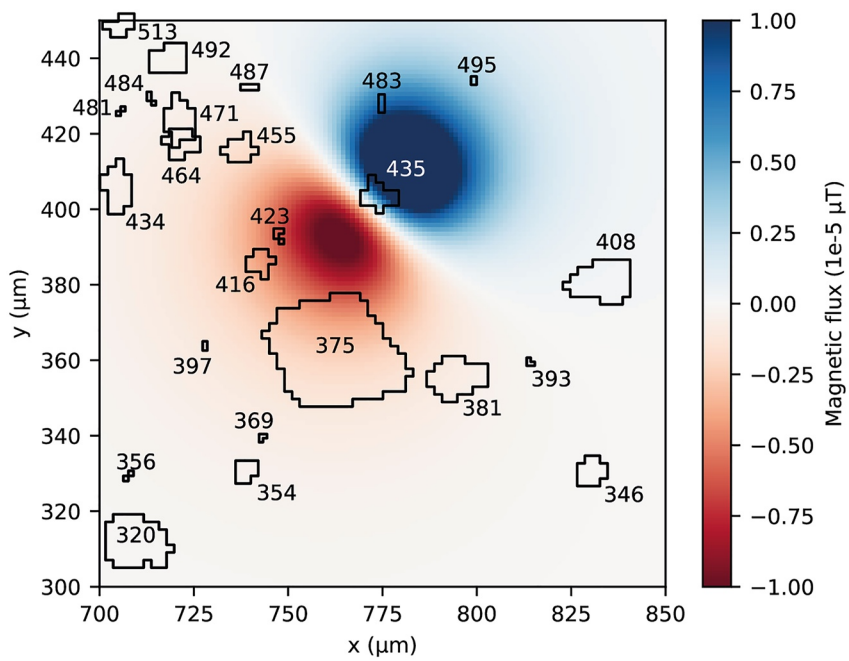

Figure 6. The forward modeled magnetic flux density map of grain 435 is present in a large part of the tile. The contributions of the other grains are removed. Note that the color scale is exaggerated with respect to the other figures in this manuscript.

ratio that can be expected for a grain, and as such an indication of how well the MMT inversion will be capable of solving its magnetic moment. Out et al. (2022) proposed to use SSR cut-offs above which MMT results can be trusted and illustrated that the SSR can be chosen such that a predefined percentage of the grains that are selected is accurately solved by MMT.

Here, we can test the performance of SSR cut-offs empirically on a natural sample for the first time.To determine the proper SSR cut-off for our data set, we have six factors to consider: (a) sample thickness, (b) domain size, (c) sampling interval, (d) grain density, (e) noise level, and (f) accepted percentage of "correctly" solved grains (Out et al., 2022). The values for sampling interval and grain density are known for our data set; the sampling interval is 1.2 μm, grain density is 3.6×10^4 grains/mm^3. The domain size for our data set is 150 μm × 150 μm and sample thickness is 30 μm. The noise level of the QDM is enigmatic: the noise is most likely Gaussian and varies for each pixel in the scan. Thus, the noise level cannot be approximated by a single value for all pixels. Based on these values, we have a choice of SSRs, because our exact case is not modeled by Out et al. (2022). We choose the SSR for the model closest to our sample, so for sample thickness of 50 μm, domain size 200 μm × 200 μm, grain density of 5.0×10^4 grains/mm^3, and sampling interval of 1 μm (Out et al., 2022, Supporting Information Figures 2a–2d). We then have a choice of modeled noise levels. As the noise level cannot be approximated by a single value for the entire scan, we choose the highest modeled noise level, 100 nT (Out et al., 2022, Supporting Information Figure 2d). We can then choose which uncertainty ratio we accept and have chosen an uncertainty ratio of 10%. These rather conservative choices lead to a SSR cutoff of $\geq 3.0 \times 10^{-3}$ μm^{-1}.

In our sample, a SSR of $\geq 3.0 \times 10^{-3}$ μm^{-1} produces a data set containing 534 grains (Figure 7b). For the directional results, the SSR $\geq 3.0 \times 10^{-3}$ μm^{-1} eliminates results over the whole range of the data set (Figure 7c). However, when comparing Figure 5b (directional scatter for all grains) and Figure 7c (directional scatter for grains with an SSR $\geq 3.0 \times 10^{-3}$ μm^{-1}) it is evident that the cut-off value does reject many grains with a high angular deviation. To assess the performance of using the SSR as cut-off further, we determined the median $\Delta\alpha$, Δm, and the precision parameter k, for the entire set of solutions (1,646 grains) and the solutions that are associated with an SSR $\geq 3.0 \times 10^{-3}$ μm^{-1} (534 grains). The median $\Delta\alpha$ changes from 25.0° to 17.0°, the median Δm goes from 22.7% to 15.3%, and the median k changes from 4.17 to 9.10. This illustrates that the SSR cut-off indeed selects grains that exhibit a more stable behavior in the inversions of the different tiles in which it is included, and that the SSR is a powerful tool to scrutinize MMT results from natural samples.

5.6. Paleomagnetic Interpretation

The paleomagnetic potential of MMT is based on the assumption that a certain subset of grains in a sample contains a reliable remanent signal that is indicative of the past state of Earth's magnetic field. Beyond SD grains, for which (Berndt et al., 2016) provided important boundary conditions, it is enigmatic which grains are reliable recorders of the paleofield and if so, how many such grains are necessary to provide a meaningful statistical ensemble for a paleomagnetic interpretation. Grains in the PSD realm (<1 μm) get increasingly more attention as possible stable recorders because of their potential vortex states (e.g., Nagy et al., 2017, 2019). MD grains are often regarded as unreliable recorders over (geologic) time scales (e.g., de Groot et al., 2014); however, recently (Berndt & Chang, 2018) argued that some MD grains may hold some potential as paleomagnetic recorders and are important to investigate for cases in which only MD grains are present (e.g., lunar samples (Wieczorek et al., 2022)). The detection limit of the MicroCT scan used here (>1.5–2 μm) only allows to characterize large, MD, grains in our sample. This implies that we miss gains that are of SD or PSD nature—the grains that are often believed to be more reliably recorders of the Earth's paleofield—in our study. In future studies, the resolution of the MicroCT scan must be lowered by approximately one order of magnitude before a meaningful paleomagnetic interpretation of MMT results will be possible. Technically, resolutions <500 μm are already achievable in NanoCT/MicroCT scans, but such scans have a limited field-of-view, lowering the amount of grains in the scan. Therefore, the "sweet-spot" in the trade-off between field-of-view and MicroCT resolution should be determined by the research question and the physical characteristics of the sample material to optimize the paleomagnetic interpretation of MMT results.

Although an interpretation in paleomagnetic terms is not possible, we can use the MMT solutions of the grains that have a SSR $\geq 3.0 \times 10^{-3}$ μm^{-1} to calculate their dispersion in directions. Since all grains analyzed in our study underwent the same magnetic history since solidification, their magnetizations are expected to be the result of the same external magnetic field(s). Their magnetic dispersion therefore gives a first-order estimate of how

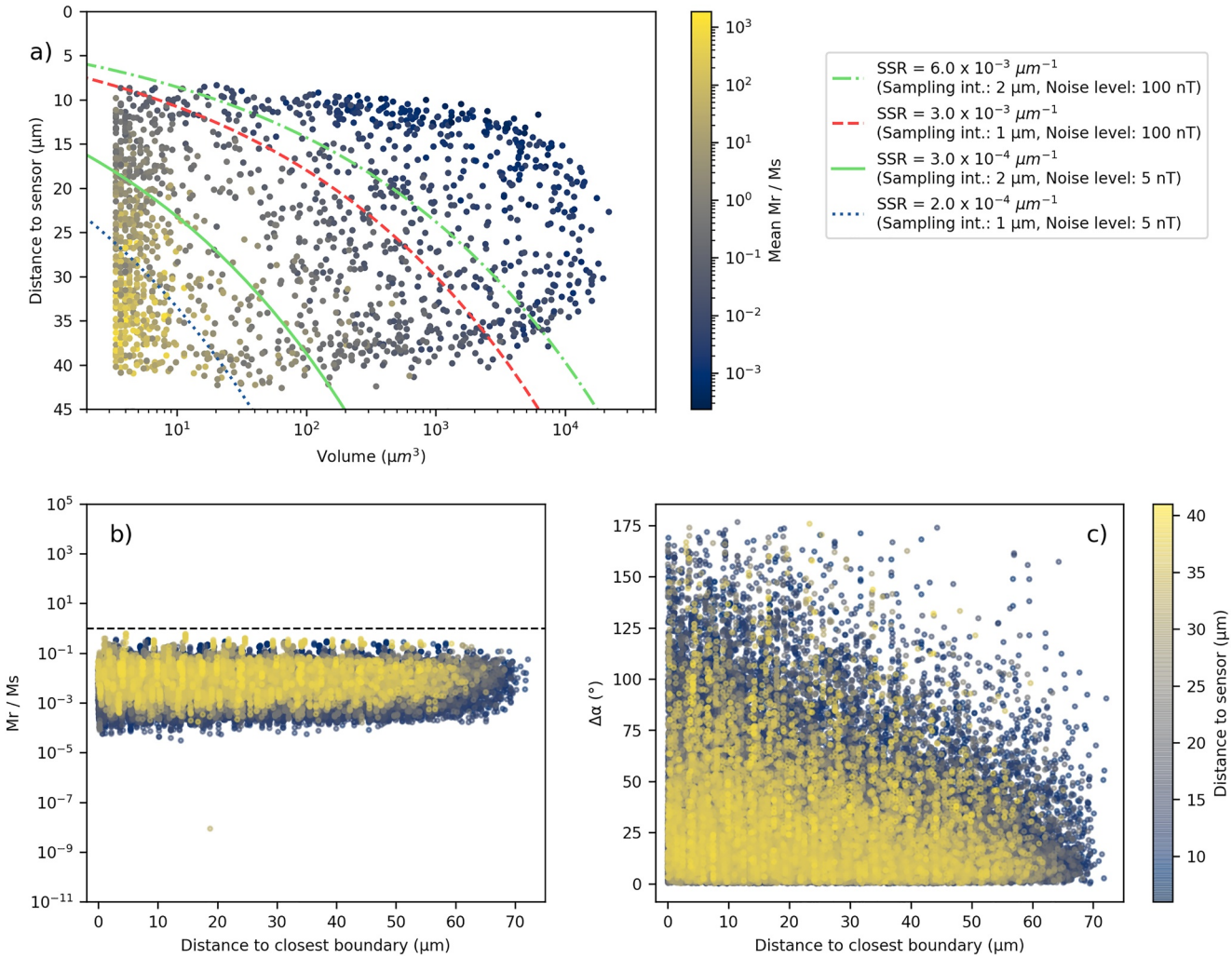

Figure 7. The signal strength ratio (SSR) is a powerful tool to select Micromagnetic Tomography. In panel (a), the M_r/M_s ratio for each grain present in the sample is indicated as a function of its volume and depth in the sample; four SSR cut-offs are indicated and show which grains are selected. The grains with a SSR $\geq 3 \times 10^{-3}$ µm^{-1} are in panels (b and c); the M_r/M_s ratio (b); and ΔAngle (c) are given as functions of distance to the closest boundary and color coded by their depth in the sample. Panels (b and c) are similar to panels (a and b) in Figure 5, but only show data points with a SSR $\geq 3 \times 10^{-3}$ µm^{-1}.

many large, MD, grains would be necessary to produce a consistent paleomagnetic direction. The Fisher mean for the 534 grains with a SSR $\geq 3.0 \times 10^{-3}$ µm^{-1} gives a declination of 245.9° and an inclination of −49.3°, with a precision parameter k of 1.075 and confidence interval $\alpha 95$ of 22.0° (Figure 8). As the number of grains, the precision parameter and the confidence interval are related (e.g., Butler, 1992), the number of grains required to obtain a smaller confidence interval with the current precision parameter can be calculated. An uncertainty of 10° or less is often considered reliable (Berndt et al., 2016); this implies that given our k of 1.075, 2,607 grains would be required to attain a confidence interval of 10°. This is 4.8 times more than the current data set of 534 grains. Our 534 grains are produced by a scanned surface of 1.52 mm^2. To acquire data from 2,607 grains after applying our MMT inversion and SSR cut-off, a scan surface of 7.42 mm^2 would be required. This is even lower than the prediction by de Groot et al. (2021) that scanning an area of 20 mm^2 would be necessary for a "reliable" result in a volcanic sample, although it must be emphasized again that the MD grains in or our analyses are most likely not reliable paleomagnetic recorders, at least not on geological timescales.

6. Conclusion

We presented a large-scale application of MMT on a natural sample producing magnetic moments of 1,646 individual grains in our sample. Due to tiling in our inversion routine, we obtained an average of 159 magnetic

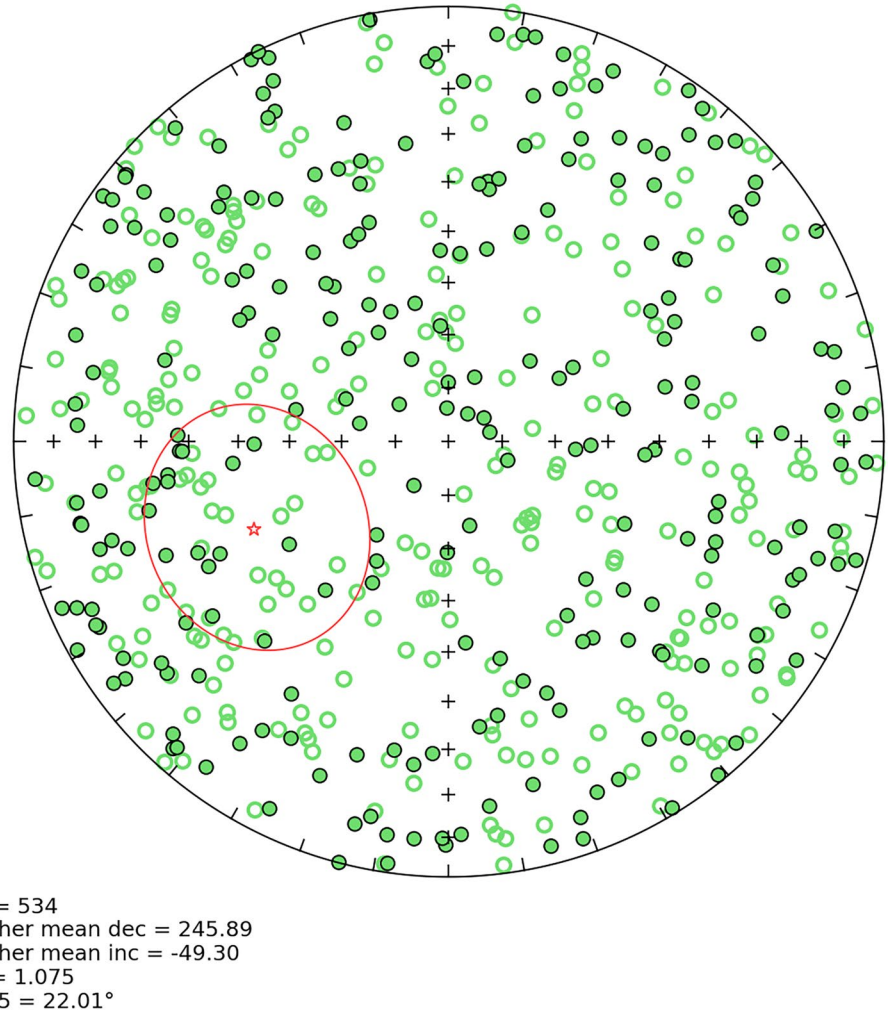

Figure 8. The mean directions of 534 grains with a signal strength ratio $\geq 3 \times 10^{-3}$ μm^{-1} in an equal area projection; closed symbols are in the lower hemisphere corresponding to positive inclinations, open symbols are in the upper hemisphere with negative inclinations. The Fisher mean of these grains is indicated by a red star, together with its 95% confidence interval as red line.

moments for each grain, so our study produced 261,305 magnetic moments in total. This enabled a statistical assessment of the results using the recently proposed SSR. After selecting the most reliable MMT results using a SSR cut-off of 3.0×10^{-3} μm^{-1}, we obtained robust results for 534 rather large and/or very shallow grains in our sample. Previous MMT studies produced magnetic moments for <150 grains. We therefore gain one order of magnitude in the number of grains that were analyzed and more than three orders of magnitude in the number of unique magnetic moments that were obtained in a single MMT study. The most important recommendation that arises from our findings is that samples for MMT studies should be smaller than the sample with a diameter of 3 mm that we used here. If the diameter of the sample would be in the order of 1 mm, it would be possible to (a) measure the magnetic flux density map of the entire surface in one QDM scan, and (b) fit the sample in the field-of-view of MicroCT scanners with resolutions <500 nm. This would imply that we could determine the magnetic moments of smaller (<1 μm) grains that may exhibit PSD behavior and are therefore better paleomagnetic recorders than the MD grains we currently can analyze. Also, if a better optimization of the MMT inversion would allow to invert the magnetic flux density map of such a 1 mm sample at once, we would satisfy the boundary condition of the MMT inversion theory that all, but only, magnetizations arising from the sources in the sample must be measured. This would remove the need for tiling during the MMT analyses and undoubtedly lead to better MMT results. Nevertheless, our study is an important step toward making MMT a useful paleomagnetic and rock-magnetic technique.

Conflict of Interest

The authors declare no conflicts of interest relevant to this study.

Data Availability Statement

The data used in this study has been uploaded to the Pangaea and can be found under https://doi.org/10.1594/PANGAEA.955725 (Kosters et al., 2023).

Acknowledgments
The authors thank Thomas Berndt and Ramon Egli for their thorough and constructive reviews, which greatly helped to improve this manuscript. This project has received funding from the European Research Council (ERC) under the European Union's Horizon 2020 research and innovation program (Grant 851460 "MIMATOM" to LVdG). LVdG acknowledges funding from the Dutch Science Foundation (NWO) Grant ALWOP.641.

References

Almeida, T. P., Muxworthy, A. R., Kovács, A., Williams, W., Brown, P. D., & Dunin-Borkowski, R. E. (2016). Direct visualization of the thermomagnetic behavior of pseudo-single-domain magnetite particles. *Science Advances*, *2*(4), e1501801. https://doi.org/10.1126/sciadv.1501801

Berndt, T., & Chang, L. (2018). Theory of stable multidomain thermoviscous remanence based on repeated domain wall jumps. *Journal of Geophysical Research: Solid Earth*, *123*(12), 10399–10417. https://doi.org/10.1029/2018JB016816

Berndt, T., Muxworthy, A. R., & Fabian, K. (2016). Does size matter? Statistical limits of paleomagnetic field reconstruction from small rock specimens. *Journal of Geophysical Research: Solid Earth*, *121*(1), 15–26. https://doi.org/10.1002/2015JB012441

Butler, R. F. (1992). *Paleomagnetism: Magnetic domains to Geologic Terranes*. Blackwell Scientific Publications.

Cortés-Ortuño, D., Fabian, K., & de Groot, L. V. (2021). Single particle multipole expansions from micromagnetic tomography. *Geochemistry, Geophysics, Geosystems*, *22*(4), e2021GC009663. https://doi.org/10.1029/2021GC009663

de Groot, L. V., Biggin, A. J., Dekkers, M. J., Langereis, C. G., & Herrero-Bervera, E. (2013). Rapid regional perturbations to the recent global geomagnetic decay revealed by a new Hawaiian record. *Nature Communications*, *4*(1), 2727. https://doi.org/10.1038/ncomms3727

de Groot, L. V., Fabian, K., Bakelaar, I. A., & Dekkers, M. J. (2014). Magnetic Force microscopy reveals meta-stable magnetic domain states that prevent reliable absolute palaeointensity experiments. *Nature Communications*, *5*(1), 4548. https://doi.org/10.1038/ncomms5548

de Groot, L. V., Fabian, K., Béguin, A., Kosters, M. E., Cortés-Ortuño, D., Fu, R. R., et al. (2021). Micromagnetic tomography for paleomagnetism and rock-magnetism. *Journal of Geophysical Research: Solid Earth*, *126*(10), 1–21. https://doi.org/10.1029/2021JB022364

de Groot, L. V., Fabian, K., Béguin, A., Reith, P., Barnhoorn, A., & Hilgenkamp, H. (2018). Determining individual particle magnetizations in assemblages of micrograins. *Geophysical Research Letters*, *45*(7), 2995–3000. https://doi.org/10.1002/2017GL076634

Dunlop, D. J., & Özdemir, Ö. (1997). *Rock magnetism*. Cambridge University Press. https://doi.org/10.1017/CBO9780511612794

Egli, R., & Heller, F. (2000). High-resolution imaging using a high-T_c superconducting quantum interference device (SQUID) magnetometer. *Journal of Geophysical Research*, *105*(B11), 25709–25727. https://doi.org/10.1029/2000jb900192

Fabian, K., & de Groot, L. V. (2019). A uniqueness theorem for tomography-assisted potential-field inversion. *Geophysical Journal International*, *216*(2), 760–766. https://doi.org/10.1093/gji/ggy455

Farchi, E., Yael Ebert, D. F., Haim, G., Shaar, R., & Bar-Gill, N. (2017). Quantitative vectorial magnetic imaging of multi-domain rock forming minerals using nitrogen-vacancy centers in diamond. *Spin*, *07*(03), 1740015. https://doi.org/10.1142/S201032471740015X

Feinberg, J. M., Harrison, R. J., Kasama, T., Dunin-Borkowski, R. E., Scott, G. R., & Renne, P. R. (2006). Effects of internal mineral structures on the magnetic remanence of silicate-hosted titanomagnetite inclusions: An electron holography study. *Journal of Geophysical Research*, *111*(12), 1–11. https://doi.org/10.1029/2006JB004498

Fisher, R. A. (1953). Dispersion on a sphere. *Proceedings of the Royal Society A: Mathematical, Physical & Engineering Sciences*, *217*(1130), 295–305. https://doi.org/10.1098/rspa.1953.0064

Fu, R. R., Lima, E. A., Volk, M. W. R., & Trubko, R. (2020). High-sensitivity moment magnetometry with the quantum diamond microscope. *Geochemistry, Geophysics, Geosystems*, *21*(8), 1–17. https://doi.org/10.1029/2020GC009147

Glenn, D. R., Fu, R. R., Kehayias, P., Le Sage, D., Lima, E. A., Weiss, B. P., & Walsworth, R. L. (2017). Micrometer-scale magnetic imaging of geological samples using a quantum diamond microscope. *Geochemistry, Geophysics, Geosystems*, *18*(8), 3254–3267. https://doi.org/10.1002/2017GC006946

Harrison, R. J., Dunin-Borkowski, R. E., & Putnis, A. (2002). Direct imaging of nanoscale magnetic interactions in minerals. *Proceedings of the National Academy of Sciences of the United States of America*, *99*(26), 16556–16561. https://doi.org/10.1073/pnas.262514499

Kosters, M. E., de Boer, R. A., Out, F., Cortés-Ortuño, D. I., & de Groot, L. V. (2023). *Magnetic surface flux data and spatial information of magnetic grains from a Hawaiian lava and results of using this data for micromagnetic tomography*. Pangaea. https://doi.org/10.1594/PANGAEA.955725

Levine, E. V., Turner, M. J., Kehayias, P., Hart, C. A., Langellier, N., Trubko, R., et al. (2019). *Principles and techniques of the quantum diamond microscope*. ArXiv.

Lima, E. A., & Weiss, B. P. (2009). Obtaining vector magnetic field maps from single-component measurements of geological samples. *Journal of Geophysical Research*, *114*(B6), B06102. https://doi.org/10.1029/2008JB006006

Lima, E. A., & Weiss, B. P. (2016). Ultra-high sensitivity moment magnetometry of geological samples using magnetic microscopy. *Geochemistry, Geophysics, Geosystems*, *17*(9), 3754–3774. https://doi.org/10.1002/2016GC006487

Nagy, L., Williams, W., Muxworthy, A. R., Fabian, K., Almeida, T. P., Conbhuí, P. Ó., & Shcherbakov, V. P. (2017). Stability of equidimensional pseudo–single-domain magnetite over billion-year timescales. *Proceedings of the National Academy of Sciences*, *114*(39), 10356–10360. https://doi.org/10.1073/pnas.1708344114

Nagy, L., Williams, W., Tauxe, L., & AdrianMuxworthy, R. (2019). From nano to micro: Evolution of magnetic domain structures in multi-domain magnetite. *Geochemistry, Geophysics, Geosystems*, *20*(May), 1–12. https://doi.org/10.1029/2019gc008319

Nichols, C. I. O., Bryson, J. F. J., Herrero-Albillos, J., Kronast, F., Nimmo, F., & Harrison, R. J. (2016). Pallasite paleomagnetism: Quiescence of a core dynamo. *Earth and Planetary Science Letters*, *441*(May), 103–112. https://doi.org/10.1016/j.epsl.2016.02.037

Out, F., Cortés-Ortũno, D., Fabian, K., Leeuwen, T., & Groot, L. V. (2022). A first-order statistical exploration of the mathematical limits of micromagnetic tomography. *Geochemistry, Geophysics, Geosystems*, *23*(4), e2021GC010184. https://doi.org/10.1029/2021gc010184

Readman, P. W., & O'Reilly, W. (1972). Magnetic properties of oxidized (cation-deficient) titanomagnetites (Fe, Ti, □)$_3$O$_4$. *Journal of Geomagnetism and Geoelectricity*, *24*(1), 69–90. https://doi.org/10.5636/jgg.24.69

Sakellariou, A., Sawkins, T. J., Senden, T. J., & Limaye, A. (2004). X-ray tomography for mesoscale physics applications. *Physica A: Statistical Mechanics and its Applications*, *339*(1–2), 152–158. https://doi.org/10.1016/j.physa.2004.03.055

Tauxe, L., & Yamazaki, T. (2015). Paleointensities. In *Treatise on geophysics* (pp. 461–509). Elsevier. https://doi.org/10.1016/B978-0-444-53802-4.00107-X

ter Maat, G. W., Pennock, G. M., & de Groot, L. V. (2018). Data descriptor: A chemical, crystallographic and magnetic characterisation of individual iron-oxide grains in Hawaiian lavas. *Scientific Data*, *5*, 1–9. https://doi.org/10.1038/sdata.2018.162

Weiss, B. P., Lima, E. A., Fong, L. E., & Baudenbacher, F. J. (2007). Paleomagnetic analysis using SQUID microscopy. *Journal of Geophysical Research*, *112*(9), B09105. https://doi.org/10.1029/2007JB004940

Wieczorek, M. A., Weiss, B. P., Breuer, D., Cébron, D., Fuller, M., Garrick-Bethell, I., et al. (2022). Lunar magnetism. Retrieved from https://hal.ird.fr/OCA/hal-03524536v1